

Chirality in odd- A Rh isotopes within triaxial particle rotor model

B. Qi,¹ S.Q. Zhang,^{2,*} S.Y. Wang,¹ J. Meng,^{3,2,4} and T. Koike⁵

¹*School of Space Science and Physics,*

Shandong University at Weihai, Weihai 264209, China

²*State Key Laboratory of Nuclear Physics and Technology,
School of Physics, Peking University, 100871 Beijing, China*

³*School of Physics and Nuclear Energy Engineering,
Beihang University, Beijing 100191, China*

⁴*Department of Physics, University of Stellenbosch, Stellenbosch, South Africa*

⁵*Department of Physics, Tohoku University, Sendai 980-8578, Japan*

(Dated: November 8, 2018)

Abstract

Adopting the fully quantal triaxial particle rotor model, the candidate chiral doublet bands in odd- A nuclei ^{103}Rh and ^{105}Rh with $\pi g_{9/2}^{-1} \otimes \nu h_{11/2}^2$ configuration are studied. For the doublet bands in both nuclei, agreement is excellent for the observed energies over entire spin range and $B(M1)/B(E2)$ at higher spin range. The evolution of the chiral geometry with angular momentum is discussed in detail by the angular momentum components and their probability distributions. Chirality is found to change from chiral vibration to nearly static chirality at spin $I = 37/2$ and back to another type of chiral vibration at higher spin. The influence of the triaxial deformation γ is also studied.

PACS numbers: 21.60.Ev, 21.10.Re, 23.20.Lv

*e-mail: sqzhang@pku.edu.cn

I. INTRODUCTION

Since the theoretical prediction of spontaneous chiral symmetry breaking in nuclear structure in 1997 [1], much effort has been devoted to further explore this interesting phenomenon. So far, more than 20 candidate chiral nuclei have been reported experimentally in the $A \sim 100, 130$ and 190 mass regions [2–17]. An overview of these studies and open problems in understanding the nuclear chirality is introduced in Ref. [18].

Of particular interest is Rh isotope chain, which has attracted significant attentions. Not only in odd-odd ^{102}Rh [13], ^{104}Rh [14], ^{106}Rh [15], but also in odd- A ^{103}Rh [13] and ^{105}Rh [16], the existence of chiral doublet bands has been claimed, while lifetime measurements for candidate chiral bands in $^{103,104}\text{Rh}$ have been performed using the recoil distance Doppler-shift method [19]. The corresponding quasiparticle configurations are suggested as $\pi g_{9/2}^{-1} \otimes \nu h_{11/2}$ for odd-odd isotopes and $\pi g_{9/2}^{-1} \otimes \nu h_{11/2}^2$ for odd- A isotopes. In particular, the candidate chiral bands in neighboring four nuclei $^{102,103,104,105}\text{Rh}$ have been regarded as a special quartet of nuclear chirality [13]. The study on this quartet permits us to investigate the detail influence on the nuclear chirality of valence nucleon configurations and inert core and to testify the validity of the theoretical approaches.

On the theoretical side, various approaches have been applied to study the nuclear chirality in Rh isotopes [18, 20, 21]. Three-dimensional tilted axis cranking (TAC) approximation [22] has been performed for the doublet bands with $\pi g_{9/2}^{-1} \otimes \nu h_{11/2}^2$ configuration in ^{105}Rh , and the aplanar solutions are obtained at relatively high rotation frequencies [16]. Using the quantal particle-rotor model (PRM), in which two quasiparticles are coupled to a triaxial core [23], the observed energy spectra, energy staggering parameter, and electromagnetic transition ratios of the candidate chiral doublet bands in ^{106}Rh were well reproduced, which supports their chiral interpretation [24]. Furthermore, the adiabatic and configuration-fixed constrained triaxial relativistic mean field approaches have been applied to study the quasiparticle configurations and the corresponding triaxial deformation in ^{106}Rh [25] as well as other Rh isotopes [26], and an interesting phenomenon, multiple chiral bands (M χ D), is suggested in $^{104,106,108,110}\text{Rh}$. The prediction of M χ D has been further examined by including time-odd fields in relativistic mean field [27].

However, for odd- A nuclei ^{103}Rh [13] and ^{105}Rh [16], the lack of nuclear model capable of addressing their doublet band separations has prevented the previous observation [13] from

being compared quantitatively with expectations for the chiral scenario. Such quantitative comparison for the separations between doublet bands can be carried out by either triaxial PRM with n -particle- n -hole configurations [28] or random phase approximation (RPA) calculations based on TAC mean field [29]. The triaxial n -particle- n -hole PRM was recently developed and has been applied to study the nuclear chirality in odd- A nucleus ^{135}Nd [28]. For the chiral doublet bands in ^{135}Nd , the observed energies and the electromagnetic transitions are reproduced excellently, and chirality is found to change from chiral vibration to nearly static chirality at spin $I = 39/2\hbar$ and back to another type of chiral vibration at higher spin. It is therefore interesting to further study the doublet bands in odd- A Rh isotopes in the framework of the fully quantal 2-particle-1-hole coupled to triaxial rotor model, which could compare experimental data quantitatively with expectations for the chiral scenario and would shed a new light on the study of nuclear chirality.

In this paper, the candidate chiral doublet bands in odd- A nuclei $^{103,105}\text{Rh}$ will be studied via a triaxial n -particle- n -hole PRM. The energy spectra and the electromagnetic transition ratios of the doublet bands in $^{103,105}\text{Rh}$ will be calculated and compared with the available data. Their chiral geometry will be discussed. Furthermore, we will investigate the influence of the triaxial deformation γ on the properties of the doublet bands.

II. FORMALISM

The total Hamiltonian is expressed as,

$$\hat{H} = \hat{H}_{\text{coll}} + \hat{H}_{\text{intr}}, \quad (1)$$

with the collective rotor Hamiltonian H_{coll} ,

$$\hat{H}_{\text{coll}} = \sum_{k=1}^3 \frac{\hat{R}_k^2}{2\mathcal{J}_k} = \sum_{k=1}^3 \frac{(\hat{I}_k - \hat{J}_k)^2}{2\mathcal{J}_k}, \quad (2)$$

where the indices $k = 1, 2, 3$ refer to the three principal axes of the body-fixed frame, $\hat{R}_k, \hat{I}_k, \hat{J}_k$ denote the angular momentum operators for the core, the total nucleus and the valence nucleons, respectively. The moments of inertia for irrotational flow are adopted, i.e., $\mathcal{J}_k = \mathcal{J}_0 \sin^2(\gamma - 2\pi k/3)$. The intrinsic Hamiltonian for valence nucleons is

$$\hat{H}_{\text{intr}} = \sum_{\nu} \varepsilon_{p,\nu} a_{p,\nu}^+ a_{p,\nu} + \sum_{\nu'} \varepsilon_{n,\nu'} a_{n,\nu'}^+ a_{n,\nu'}. \quad (3)$$

The single particle energy for proton $\varepsilon_{p,\nu}$ and for neutron $\varepsilon_{n,\nu'}$ are obtained by the diagonalization of the triaxial deformed single- j shell Hamiltonian [1],

$$h_{\text{sp}} = \pm \frac{1}{2} C \left\{ \cos \gamma (\hat{j}_3^2 - \frac{j(j+1)}{3}) + \frac{\sin \gamma}{2\sqrt{3}} (\hat{j}_+^2 + \hat{j}_-^2) \right\}, \quad (4)$$

where the plus or minus sign refers to particle or hole, and the coefficient C is proportional to the quadrupole deformation β as in Ref. [24].

The single particle states are expressed as

$$a_\nu^+ |0\rangle = \sum_{\alpha\Omega} c_{\alpha\Omega}^{(\nu)} |\alpha, \Omega\rangle, \quad a_{\bar{\nu}}^+ |0\rangle = \sum_{\alpha\Omega} (-1)^{j-\Omega} c_{\alpha\Omega}^{(\nu)} |\alpha, -\Omega\rangle, \quad (5)$$

where Ω is the projection of the single-particle angular momentum \hat{j} along the 3-axis and is restricted to the values $\dots, -7/2, -3/2, 1/2, \dots$, due to the time-reversal degeneracy [30], and α denotes the other quantum numbers. For a system with z valence protons and n valence neutrons, the intrinsic wave function is given as

$$|\varphi\rangle = \left(\prod_{i=1}^{z_1} a_{p,\nu_i}^\dagger \right) \left(\prod_{i=1}^{z_2} a_{p,\bar{\mu}_i}^\dagger \right) \left(\prod_{i=1}^{n_1} a_{n,\nu'_i}^\dagger \right) \left(\prod_{i=1}^{n_2} a_{n,\bar{\mu}'_i}^\dagger \right) |0\rangle \quad (6)$$

with $z_1 + z_2 = z, n_1 + n_2 = n, 0 \leq z_1 \leq z, 0 \leq n_1 \leq n$.

The total wave function can be expanded into the strong coupling basis,

$$|IM\rangle = \sum_{K\varphi} c_{K\varphi} |IMK\varphi\rangle, \quad (7)$$

with

$$|IMK\varphi\rangle = \frac{1}{\sqrt{2(1 + \delta_{K0}\delta_{\varphi,\bar{\varphi}})}} (|IMK\rangle|\varphi\rangle + (-1)^{I-K} |IM-K\rangle|\bar{\varphi}\rangle), \quad (8)$$

where $|IMK\rangle$ denotes the Wigner functions $\sqrt{\frac{2I+1}{8\pi^2}} D_{MK}^I$ and φ is a shorthand notation for the configurations in Eq. (6). The basis states are symmetrized under the point group D_2 , which leads to $K - \frac{1}{2}(z_1 - z_2) - \frac{1}{2}(n_1 - n_2)$ being an even integer with $\Omega = \dots, -3/2, 1/2, 5/2, \dots$. The detailed explanation for such a restriction is given in Appendix. The reduced transition probabilities $B(M1)$ and $B(E2)$ can be obtained from the wave function of PRM with the $M1$ and $E2$ operators [23].

III. RESULTS AND DISCUSSION

In the PRM calculations for the doublet bands in $^{103,105}\text{Rh}$, the configuration $\pi g_{9/2}^{-1} \otimes \nu h_{11/2}^2$ [13, 16] is adopted. By applying the microscopic self-consistent triaxial relativistic mean field approach [25], the deformation parameters for ground states of $^{103,105}\text{Rh}$ have been obtained with PK1 parameter set [25], i.e., $\beta = 0.235$ and $\gamma = 20.6^\circ$ for ^{103}Rh while $\beta = 0.228$ and $\gamma = 21.1^\circ$ for ^{105}Rh . Accordingly, C_p and C_n in single- j Hamiltonian (4) take values of -0.43 and 0.35 MeV for ^{103}Rh while -0.42 and 0.34 MeV for ^{105}Rh [24]. For all doublet bands investigated, the moment of inertia $\mathcal{J}_0 = 21.0$ MeV/ \hbar^2 is adjusted to the experimental energy spectra. For the electromagnetic transition, the empirical intrinsic quadrupole moment $Q_0 = (3/\sqrt{5\pi})R_0^2 Z\beta \approx 2.5$ eb, gyromagnetic ratios $g_R = Z/A = 0.44$, and $g_p(g_{9/2}) = 1.26$, $g_n(h_{11/2}) = -0.21$ are adopted. The proton and neutron g factors are determined from $g_{p(n)} = g_l + (g_s - g_l)/(2l + 1)$ with $g_l = 1(0)$ for proton (neutron) and $g_s = 0.6g_s(\text{free})$.

A. ^{103}Rh

The calculated excitation energy spectra $E(I)$ for the doublet bands (denoted by A and B) in ^{103}Rh are presented in Fig. 1, in comparison with the corresponding data available, i.e. bands 3 and 4 in Ref. [13]. The experimental energy spectra are well reproduced by the PRM calculation with an accuracy within 150 keV. In particular, the trend and amplitude of the energy separation between the doublet bands are excellently reproduced. The least energy separation between the doublet bands happens at $I = 37/2$ for both the experimental and theoretical energy spectra.

The calculated in-band $B(M1)/B(E2)$ ratios for the doublet bands in ^{103}Rh are presented in Fig. 2, together with the available data [13]. For the whole spin region, the observed in-band $B(M1)/B(E2)$ ratios in the two bands are almost the same. These features are well reproduced by the PRM calculation. No strong odd-even staggering of the $B(M1)/B(E2)$ ratios are observed in the doublet bands, as well as the PRM results. In Ref. [31], it is pointed out that this odd-even staggering associates strongly with the characters of nuclear chirality, i.e., the staggering is weak in the chiral vibration region while strong in the static chirality region based on the calculations of one particle one hole coupled with a triaxial

rotor.

Lifetime measurements for candidate chiral bands in $^{103,104}\text{Rh}$ have been performed in Ref. [19] and the $B(M1)$ and $B(E2)$ values in band A are extracted. The $B(M1)$ and $B(E2)$ values calculated by means of the PRM for the chiral doublet bands in ^{103}Rh are plotted in Fig. 3 in comparison with the data [19]. The predicted $B(E2)$ values increase smoothly as the spin increasing, while the predicted $B(M1)$ values decrease smoothly as the spin increasing. The PRM calculations well reproduce the observed $B(E2)$ values, while somewhat overestimate the observed $B(M1)$ values. Additionally, both the calculated in-band $B(M1)$ and $B(E2)$ values are much larger than the interband ones, which is consistent with the present experimental observations.

The deviation between the calculated $B(M1)$ values and the observed data may be understood by the incorporation of one quasiparticle configuration into the first several states of the observed three quasiparticles band, as one quasiparticle band gives small $B(M1)$ values. If the pairing interactions are included to treat with the mixing between one- and three-quasiparticle configurations, the observed $B(M1)$ values would be better reproduced. In addition, the dependence of the $B(M1)$ values on γ has been checked. It is found that the $B(M1)$ values of the yrast band for the lower spins have hardly changed for different γ values. The agreement between the calculated results and $B(M1)$ data does not improve much by adjusting of γ .

The success in reproducing the energy spectra and transition probabilities of the doublet bands A and B in ^{103}Rh suggests that the PRM calculation correctly accounts for the structure of the states. To exhibit their chiral geometry hold by the angular momenta, the rms values of the angular momentum components for the core $R_k = \sqrt{\langle \hat{R}_k^2 \rangle}$, the valence proton $J_{pk} = \sqrt{\langle \hat{j}_{pk}^2 \rangle}$, and the valence neutrons $J_{nk} = \sqrt{\langle (\hat{j}_{(n1)k} + \hat{j}_{(n2)k})^2 \rangle}$, are presented in Fig. 4, in which $k = i, l, s$, represent the intermediate, short and long axes respectively.

As shown in Fig. 4, for both bands A and B with spin larger than the band head $27/2\hbar$ of band B, the collective core angular momentum mainly aligns along the intermediate axis. The angular momentum of the $g_{9/2}$ valence proton hole mainly aligns along the long axis and that of the two aligned $h_{11/2}$ valence neutrons mainly along the short axis, which correspond to the orientation preferred by their interaction with the triaxial core [1]. To be more precise, $\mathbf{J}_p \sim 5\hbar$ along l -axis, and both $\mathbf{J}_n \sim 10\hbar$ and $\mathbf{R} \sim 6 - 12\hbar$ lie in the plane spanned by i - and s - axis, which together form the chiral geometry of aplanar rotation.

As the total angular momentum increases, \mathbf{R} increases gradually. Due to the Coriolis coupling and the rotational alignment, both \mathbf{J}_p and \mathbf{J}_n moves gradually toward the i -axis, the largest rotational axis. The i -component for \mathbf{J}_n increase more rapidly than that of \mathbf{J}_p , as the two aligned $h_{11/2}$ valence neutrons provide larger component on i -axis. At spin $I = 37/2$, where the doublet bands have the smallest energy difference, the orientations of \mathbf{R} , \mathbf{J}_n and \mathbf{J}_p for band A and band B are nearly identical. Hence around this spin the structure comes closest to the ideal chiral picture of a left- and a right-handed configurations with equal components \mathbf{R} , \mathbf{J}_n , and \mathbf{J}_p along the respective i -, l -, and s -axes.

It is interesting to analyze the evolution of the rms components of angular momentum before the starting of the doublet bands ($I < 27/2$). For band A, the unpairing process of two $h_{11/2}$ valence neutrons seems to happen during spin 19/2 to 23/2. Before that, the two valence neutrons are paired and contribute few angular momenta on three axes. When $I \geq 23/2$, the two $h_{11/2}$ neutrons are unpaired, which mainly align along the s -axis (towards i -axis with spin increasing) and contribute $9\hbar$. The onset of three quasiparticles configuration is pleasingly consistent with the observed band head ($I = 23/2$) of band 3 in Ref. [16]. For band B, the unpairing process is complete at spin 27/2, which is exactly the observed band head of band 4 in Ref. [16]. This observation indicates that the present calculation treats automatically and properly the angular momentum alignment of valence particles. However, as the moment of inertia is a constant in present PRM calculation, one cannot expect the simultaneous quantitative description of 1-qp and 3-qp rotational bands.

Further understanding the evolution of the chirality with angular momentum as performed for the chiral bands in ^{135}Nd in the $A \sim 130$ region similarly in Ref. [28], the probability distributions for the projection of the total angular momentum along the l -, i - and s -axes are given in Fig. 5 for the doublet bands in ^{103}Rh . For spin $I = 27/2$, near the band head, the probability distribution of two bands differs as expected for a chiral vibration. For the lower band A, the maximum probability for the i -axis appears at $K_i = 0$, whereas the probability for the higher band B is zero at $K_i = 0$, having its peak at $K_i = 19/2$. These probability distributions resemble those in the chiral vibration picture shown in TAC+RPA theory, in which the state (A) and state (B) are considered as the zero phonon and one phonon states [29]. The probability distributions with respect to the l -axis have a peak near $K_l = 9/2$, and respect to the s -axis have a peak near $K_s = 10$. Hence the chiral vibration consists in an oscillation of the collective angular momentum vector \mathbf{R} through the s - l -plane.

This reveals the structure of the chiral vibration [29].

At spin $I = 37/2$, the probability distributions for band A and B are very similar. The distributions are peaked at about $K_l = 7$, $K_i = 17$, $K_s = 16$. The well developed tunneling regime, namely the well established static chirality region, is restricted around $I = 37/2$. For higher spin, where the energy difference between the chiral doublets increases, they attain vibration character again. This is reflected by the increasing differences between the probability distributions of bands A and B. In particular the fact that $P(K_s = 0)$ is finite for band A and zero for band B shows that the motion contains a vibration of the vector \mathbf{I} through the l - i -plane.

B. ^{105}Rh

The triaxial PRM calculations have also been applied to the doublet bands with the configuration $\pi g_{9/2}^{-1} \otimes \nu h_{11/2}^2$ in ^{105}Rh , namely bands 4 and 5 in Ref. [16]. The calculated excitation energy spectra $E(I)$ for the doublet bands A and B in ^{105}Rh are presented in Fig. 6, together with the corresponding data [16]. The experimental energy spectra are well reproduced by the PRM calculation. The calculated results agree with the data within 100 keV for spin $I < 41/2$. The trend and amplitude for the energy splitting between two doublet bands are also comparable. However, there still exists certain deviation in energy splitting that the best degeneracy spin is $41/2$ for data, but $39/2$ for PRM calculation.

The calculated in-band $B(M1)/B(E2)$ ratios for the doublet bands in ^{105}Rh are presented in Fig. 7, together with the available data [13]. For the whole spin region, the observed in-band $B(M1)/B(E2)$ ratios in the two bands are similar within error bar. These features are reproduced by the PRM calculation. The small difference of magnitude can be seen in experimental data as well at large spins for PRM calculations. The staggering of the $B(M1)/B(E2)$ ratios are not obvious in this nucleus, which is consistent with the PRM calculation. The absolute $B(E2)$ and $B(M1)$ values for the doublet bands in ^{105}Rh from the PRM calculation are also plotted in Fig. 8, in order to compare with future lifetime data.

To study their chiral geometry, the rms values of the angular momentum components for the core, the valence proton and the valence neutrons, and the probability distributions of projection K of total angular momentum are also calculated, and the results are almost the same as that in ^{103}Rh . Thus the evolution of the chiral geometry with angular momentum

in ^{105}Rh are almost identical to that in ^{103}Rh . To avoid repetition, these results are not shown here.

It is interesting to note that in ^{105}Rh , a pair of negative parity bands (band 7 and 8 in Ref. [17]) have been also regarded as another chiral doublet bands [17]. The corresponding quasiparticle configuration was suggested as $\pi g_{9/2}^{-1} \otimes \nu h_{11/2}(g_{7/2}, d_{5/2})$. This fact indicates the possible experimental evidence for the existence of M χ D [25] in ^{105}Rh , namely a pair of chiral bands with positive parity and configuration $\pi g_{9/2}^{-1} \otimes \nu h_{11/2}^2$, while another pair of chiral bands with negative parity and configuration $\pi g_{9/2}^{-1} \otimes \nu h_{11/2}(g_{7/2}, d_{5/2})$. As the latter configuration involves the orbits of pseudospin doublet states $(g_{7/2}, d_{5/2})$, a competing interpretation of band 7 and 8 in Ref. [17] includes the pseudospin doublet bands [18]. Further efforts are needed to address this point.

C. The influence of γ on the doublet bands

In the previous study of chiral doublet bands in odd-odd nuclei with particle rotor model, it has been found that the triaxial deformation γ is one of the most sensitive parameters for the properties of the doublet bands [31]. Here, we made a systematic triaxial PRM calculation with configuration $\pi g_{9/2}^{-1} \otimes \nu h_{11/2}^2$, and plot the energy difference between the two lowest bands A and B and their in-band $B(M1)/B(E2)$ ratios for different triaxiality parameter γ in Fig. 9 and 10.

As shown in Fig. 9, as the γ value increases, the calculated energy difference between doublet bands decreases rapidly. The smallest energy differences are obtained at spin 37/2 for most γ values. At this point, the energy differences are 946, 693, 475, 261, 175, 79, 21, 30, 34 keV for $\gamma = 14^\circ, 16^\circ, 18^\circ, 20^\circ, 22^\circ, 24^\circ, 26^\circ, 28^\circ, 30^\circ$, respectively. It is found that around $\gamma = 20^\circ$, the calculated energy difference agrees with the data in $^{103,105}\text{Rh}$ very well.

As shown in Fig. 10, the calculated in-band $B(M1)/B(E2)$ ratios in the doublet bands are almost the same over the whole spin region for different triaxiality parameters γ . These calculated in-band $B(M1)/B(E2)$ values are sensitive to the triaxiality parameter γ . Such two pronounced features for $B(M1)/B(E2)$, i.e., the similarity between the doublet bands and the sensitivity to γ , are consistent with the features in chiral doublet bands calculated with 1-particle-1-hole coupled to triaxial rotor model in Ref. [31]. However, the staggering of the $B(M1)/B(E2)$ ratios are not obvious for $\gamma < 24^\circ$, and the staggering appear only

around spin $37/2$ for $\gamma = 26^\circ, 28^\circ, 30^\circ$, which are very different from the features in the case of 1-particle-1-hole configurations in Ref. [31].

IV. SUMMARY

In summary, adopting the particle-rotor model, which couples a triaxial rotor with one valence proton hole and two valence neutrons, the candidate chiral doublet bands with $\pi g_{9/2}^{-1} \otimes \nu h_{11/2}^2$ configuration in the odd- A Rh isotopes, ^{103}Rh and ^{105}Rh , are investigated. The agreement is excellent for the energy spectra of the doublet bands over entire spin range and in-band $B(M1)/B(E2)$ ratios at higher spin range. The absolute $B(M1)$ and $B(E2)$ transition probabilities for the doublet bands in ^{103}Rh and ^{105}Rh have been presented, which has reasonable agreement with the data available and invites further lifetime measurements in the chiral rotation region.

Both in ^{103}Rh and ^{105}Rh , the chiral doublet bands start as a chiral vibration of the angular momentum about the intermediate axis. Static chirality is reached at $I = 37/2$, where the two bands approach each other closest. After that the two bands again develop into a chiral vibration of the angular momentum about the short axis.

For the doublet bands with $\pi g_{9/2}^{-1} \otimes \nu h_{11/2}^2$ configuration, it is found that both the energy spectra difference and their in-band $B(M1)/B(E2)$ ratios are sensitive to the triaxiality parameter γ . No regular staggering of the $B(M1)/B(E2)$ ratios is found for the doublet bands with this configuration for different γ values.

Acknowledgements

This work is partly supported by the National Natural Science Foundation of China under Grant Nos. 11005069, 10975007, 10975008, 10875074, 10775004, the Independent Innovation Foundation of Shandong University (IIFSDU), and the Major State Research Development Program of China (No. 2007CB815000).

V. APPENDIX

In the appendix, we will show the restriction of the model basis Eq. (8). The model basis should be symmetrized under the D_2 point group, namely the operators $\hat{R}_1(\pi)$, $\hat{R}_2(\pi)$ and $\hat{R}_3(\pi)$ which represent rotation of 180° about the three principal axes in body-fixed frame. When the model basis is written as Eq. (8), it has been ensured that the basis is invariant under $\hat{R}_2(\pi)$ (see such as Refs. [32, 33]).

For $\hat{R}_3(\pi) = \exp[\frac{-i}{\hbar}\pi(\hat{I}_3 - \hat{j}_3)]$,

$$\hat{R}_3(\pi)a_\nu^\dagger|0\rangle = \hat{R}_3(\pi) \sum_{\alpha\Omega} c_{\alpha\Omega}^{(\nu)}|\alpha, \Omega\rangle = \sum_{\alpha\Omega} c_{\alpha\Omega}^{(\nu)}(-1)^{-\Omega}|\alpha, \Omega\rangle. \quad (9)$$

Because Ω has been restricted as $\dots, -3/2, 1/2, 5/2, \dots$ in Eq. (5),

$$R_3(\pi)a_\nu^\dagger|0\rangle = \sum_{\alpha\Omega} c_{\alpha\Omega}^{(\nu)}(-1)^{-(1/2+2*\text{integer})}|\alpha, \Omega\rangle = (-1)^{-1/2}a_\nu^\dagger|0\rangle. \quad (10)$$

Similarly, $R_3(\pi)a_{\bar{\nu}}^\dagger|0\rangle = (-1)^{1/2}a_{\bar{\nu}}^\dagger|0\rangle$. Hence, when $\hat{R}_3(\pi)$ operates on the intrinsic wave function, we get

$$\begin{aligned} R_3(\pi)|\varphi\rangle &= R_3(\pi) \left(\prod_{i=1}^{z_1} a_{p,\nu_i}^\dagger \right) \left(\prod_{i=1}^{z_2} a_{p,\bar{\mu}_i}^\dagger \right) \left(\prod_{i=1}^{n_1} a_{n,\nu'_i}^\dagger \right) \left(\prod_{i=1}^{n_2} a_{n,\bar{\mu}'_i}^\dagger \right) |0\rangle \\ &= (-1)^{-\frac{1}{2}z_1} (-1)^{\frac{1}{2}z_2} (-1)^{-\frac{1}{2}n_1} (-1)^{\frac{1}{2}n_2} |\varphi\rangle. \end{aligned} \quad (11)$$

Consequently,

$$R_3(\pi)|IMK\rangle|\varphi\rangle = (-1)^{K-\frac{1}{2}(z_1-z_2)-\frac{1}{2}(n_1-n_2)}|IMK\rangle|\varphi\rangle; \quad (12)$$

$$R_3(\pi)|IM-K\rangle|\bar{\varphi}\rangle = (-1)^{-K+\frac{1}{2}(z_1-z_2)+\frac{1}{2}(n_1-n_2)}|IM-K\rangle|\bar{\varphi}\rangle. \quad (13)$$

To ensure the model basis $|IMK\rangle|\varphi\rangle$ in Eq. (8) is symmetrized under $\hat{R}_3(\pi)$, $K - \frac{1}{2}(z_1 - z_2) - \frac{1}{2}(n_1 - n_2)$ must be an even integer.

According to the group theory, if the model basis $|IMK\rangle|\varphi\rangle$ is symmetrized under $\hat{R}_2(\pi)$ and $\hat{R}_3(\pi)$, it can be ensured that the basis is also symmetrized under $\hat{R}_1(\pi)$, namely symmetrized under the D_2 point group.

[1] S. Frauendorf and J. Meng, Nucl. Phys. **A617**, 131 (1997).

[2] K. Starosta *et al.*, Phys. Rev. Lett. **86**, 971 (2001).

- [3] T. Koike, K. Starosta, C. J. Chiara, D. B. Fossan, and D. R. LaFosse, Phys. Rev. C **63**, 061304(R) (2001).
- [4] R. A. Bark, *et al.*, Nucl. Phys. **A691**, 577 (2001).
- [5] E. Mergel *et al.*, Eur. Phys. J. **A15**, 417 (2002).
- [6] T. Koike, K. Starosta, C. J. Chiara, D. B. Fossan, and D. R. LaFosse, Phys. Rev. C **67**, 044319 (2003).
- [7] S. Zhu *et al.*, Phys. Rev. Lett. **91**, 132501 (2003).
- [8] S. Y. Wang, Y. Z. Liu, T. Komatsubara, Y. J. Ma, and Y. H. Zhang, Phys. Rev. C **74**, 017302 (2006).
- [9] E. Grodner *et al.*, Phys. Rev. Lett. **97**, 172501 (2006).
- [10] D. Tonev *et al.*, Phys. Rev. Lett. **96**, 052501 (2006)
- [11] P. Joshi *et al.*, Phys. Rev. Lett. **98**, 102501(2007).
- [12] E. A. Lawrie *et al.*, Phys. Rev. C **78**, 021305(R) (2008).
- [13] J. Timár, *et al.*, Phys. Rev. C **73**, 011301(R) (2006).
- [14] C. Vaman, D. B. Fossan, T. Koike, K. Starosta, I. Y. Lee, and A. O. Macchiavelli, Phys. Rev. Lett. **92**, 032501 (2004).
- [15] P. Joshi *et al.*, Phys. Lett. **B595**, 135 (2004).
- [16] J. Timár *et al.*, Phys. Lett. **B598**, 178 (2004).
- [17] J. A. Alcántara-Núñez *et al.*, Phys. Rev. C **69**, 024317 (2004).
- [18] J. Meng and S. Q. Zhang, J. Phys. G **37**, 064025 (2010).
- [19] T. Suzuki *et al.* Phys. Rev. C **78**, 031302(R) (2008).
- [20] S. Frauendorf, Rev. Mod. Phys. **73**, 463 (2001).
- [21] J. Meng, B. Qi, S.Q. Zhang and S.Y. Wang, Mod. Phys. A **23**, 2560 (2008).
- [22] V. I. Dimitrov, S. Frauendorf, and F. Dönau, Phys. Rev. Lett. **84**, 5732 (2000).
- [23] S. Q. Zhang, B. Qi, S. Y. Wang, and J. Meng, Phys. Rev. C **75**, 044307 (2007).
- [24] S. Y. Wang, S. Q. Zhang, B. Qi, J. Peng, J. M. Yao, and J. Meng, Phys. Rev. C **77**, 034314 (2008).
- [25] J. Meng, J. Peng, S. Q. Zhang, and S.-G. Zhou, Phys. Rev. C **73**, 037303 (2006).
- [26] J. Peng, H. Sagawa, S. Q. Zhang, J M Yao, Y Zhang, and J. Meng Phys. Rev. C **77**, 024309 (2008).
- [27] J. M. Yao, B. Qi, S. Q. Zhang, J. Peng, S. Y. Wang and J. Meng Phys. Rev. C **79**, 067302

(2009)

- [28] B. Qi, S. Q. Zhang, J. Meng, and S. Frauendorf, Phys. Lett. B, **675**, 175 (2009).
[29] S. Mukhopadhyay *et al.*, Phys. Rev. Lett. **99**, 172501 (2007).
[30] S. E. Larsson, G. Leander, and I. Ragnarsson, Nucl. Phys. A **307**, 189 (1978).
[31] B. Qi, S. Q. Zhang, S. Y. Wang, J.M. Yao and J. Meng, Phys. Rev. C **79**, 041302(R) (2009)
[32] I. Ragnarsson and P. B. Semmes, Hyp. Int. **43**, 425 (1988)
[33] B. G. Carlsson, I. Ragnarsson, Phys. Rev. C **74**, 044310 (2006)

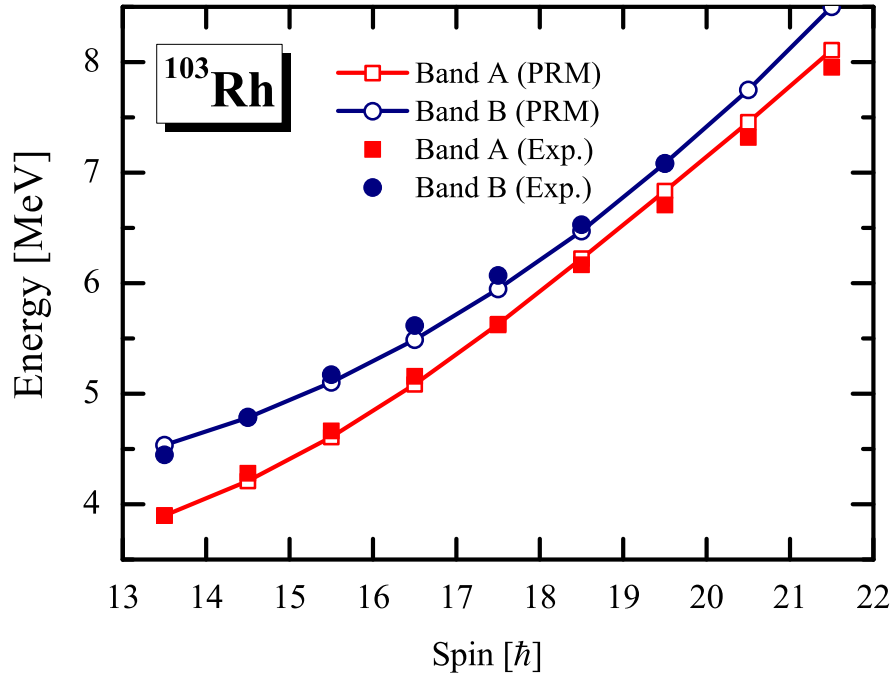


FIG. 1: (color online) The energies $E(I)$ for the chiral doublet bands in ^{103}Rh calculated by the triaxial PRM with configuration $\pi g_{9/2}^{-1} \otimes \nu h_{11/2}^2$ (open symbols connected by full line) in comparison with the data (filled symbols) [13].

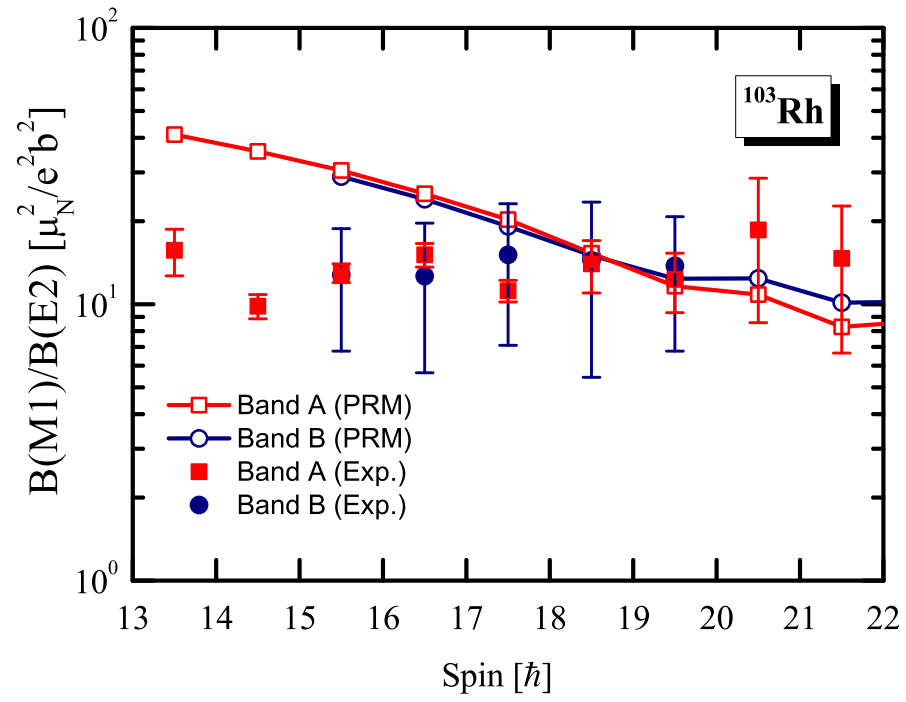


FIG. 2: (color online) The $B(M1)/B(E2)$ values calculated by PRM for the chiral doublet bands in ^{103}Rh (open symbols connected by full line) in comparison with the data (filled symbols) [13].

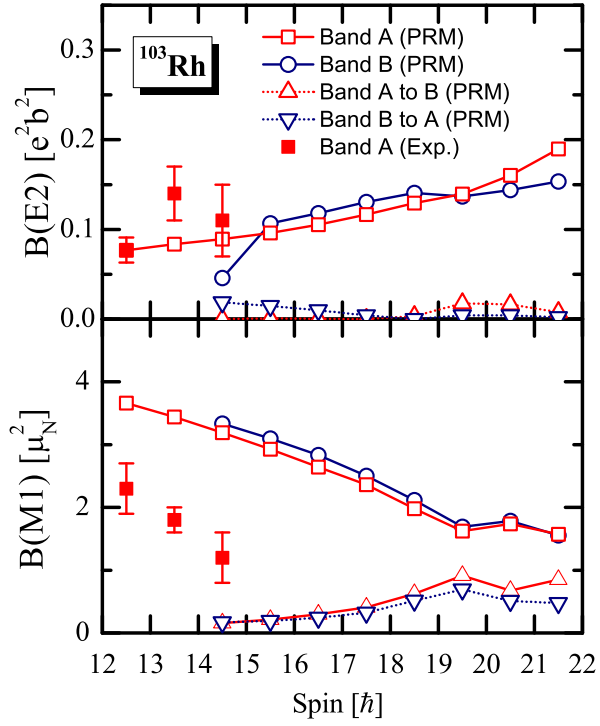


FIG. 3: (color online) The $B(M1)$ and $B(E2)$ values calculated by PRM for the chiral doublet bands in ^{103}Rh (open symbols) in comparison with the data available (filled symbols) [19].

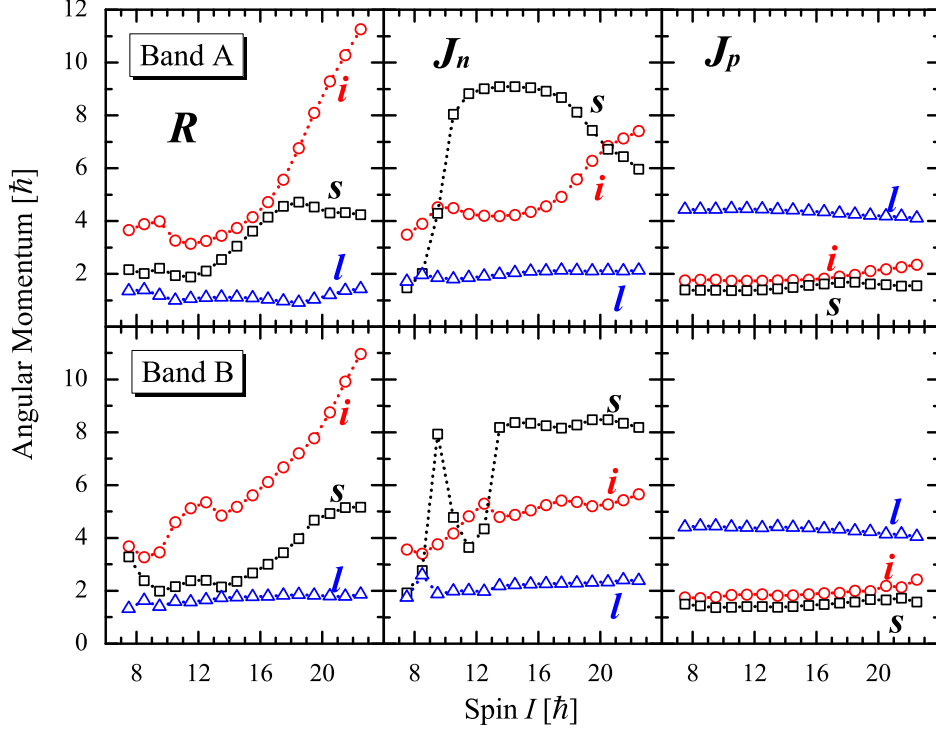


FIG. 4: (color online) The root mean square components along the intermediate (i -, circles), short (s -, squares) and long (l -, triangles) axis of the core $R_k = \sqrt{\langle \hat{R}_k^2 \rangle}$, valence proton $J_{pk} = \sqrt{\langle \hat{j}_{pk}^2 \rangle}$, and valence neutrons angular momenta $J_{nk} = \sqrt{\langle (\hat{j}_{(n1)k} + \hat{j}_{(n2)k})^2 \rangle}$ calculated as functions of spin I by means of the PRM for the doublet bands in ^{103}Rh .

FIG. 5: (color online) The probability distributions for projection of total angular momentum on the long (l -), intermediate (i -) and short (s -) axis in PRM for the doublet bands in ^{103}Rh .

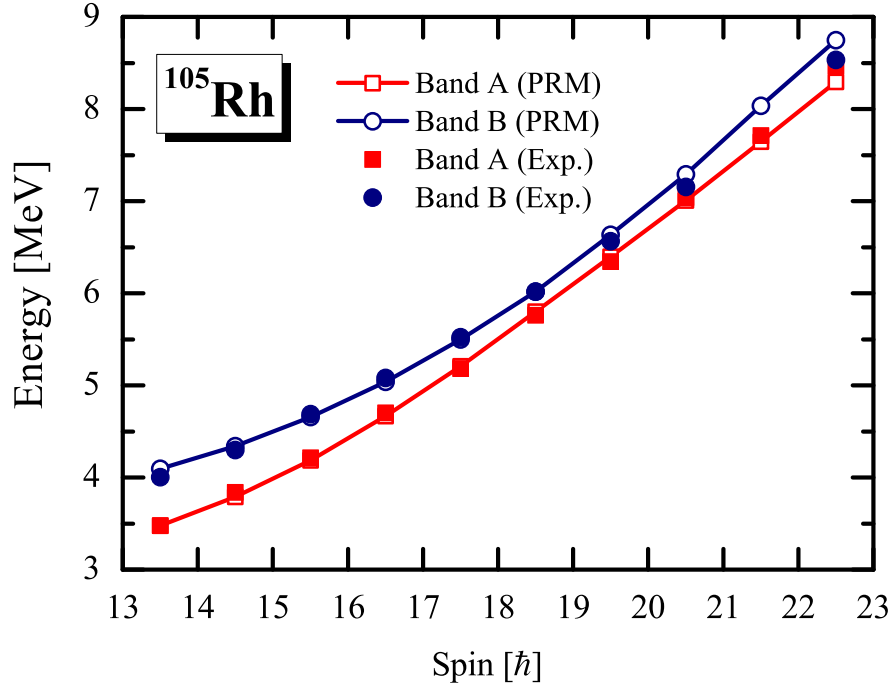


FIG. 6: (color online) The energies $E(I)$ for the chiral doublet bands in ^{105}Rh calculated by the triaxial PRM with configuration $\pi g_{9/2}^{-1} \otimes \nu h_{11/2}^2$ (open symbols connected by full line) in comparison with the data (filled symbols) [16, 17].

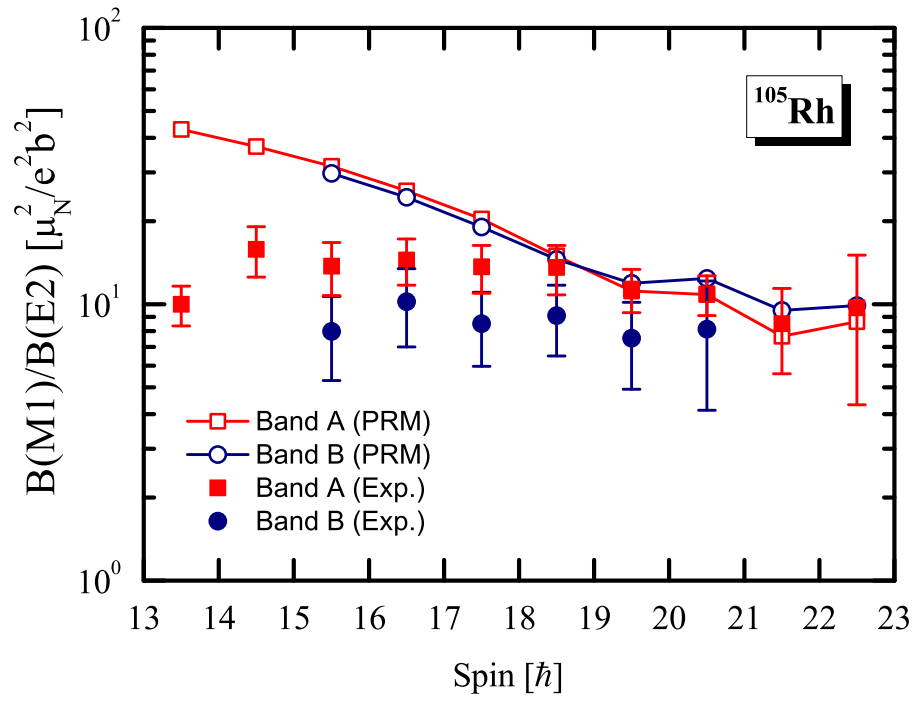


FIG. 7: (color online) The $B(M1)/B(E2)$ values calculated by PRM for the chiral doublet bands in ^{105}Rh (open symbols connected by full line) in comparison with the data (filled symbols) [16, 17].

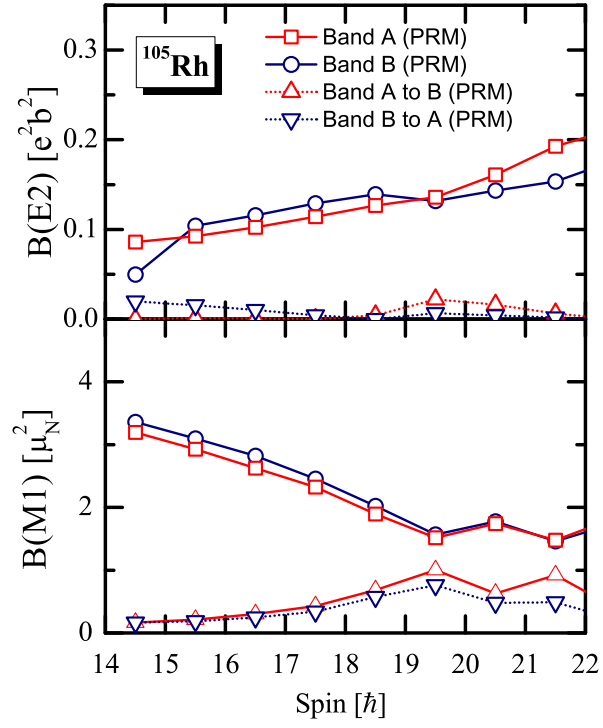


FIG. 8: (color online) The $B(M1)$ and $B(E2)$ values calculated by PRM for the chiral doublet bands in ^{105}Rh .

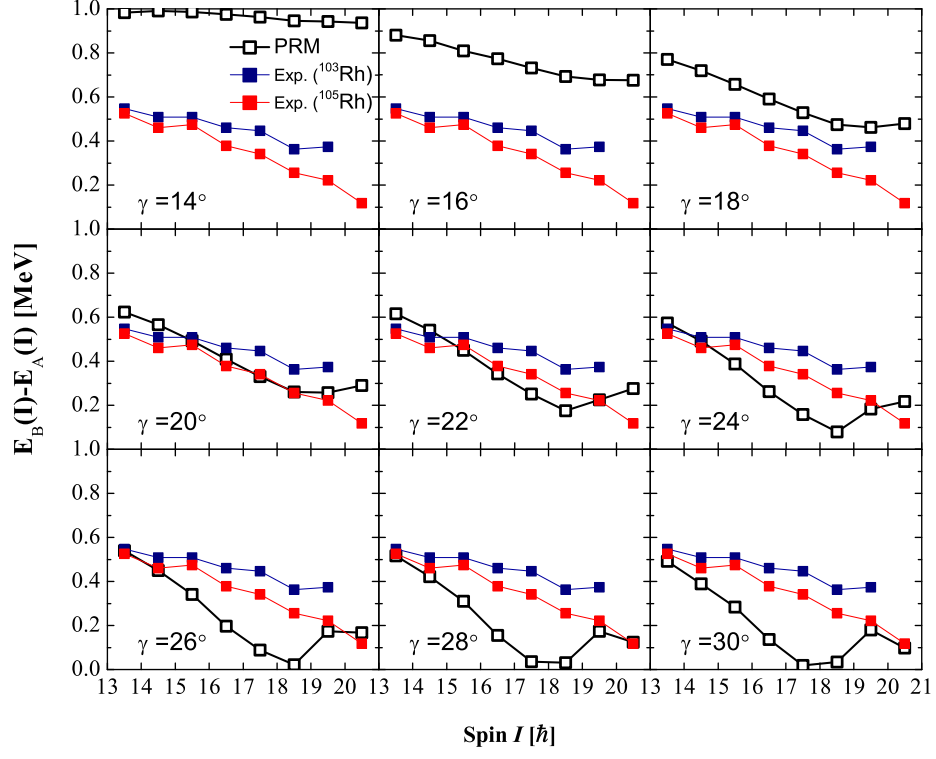


FIG. 9: (color online) Energy difference between the two lowest bands A and B calculated in PRM with different triaxiality parameters γ with configuration $\pi g_{9/2}^{-1} \otimes \nu h_{11/2}^2$ (open symbols) in comparison with the data of ^{103}Rh and ^{105}Rh (filled symbols).

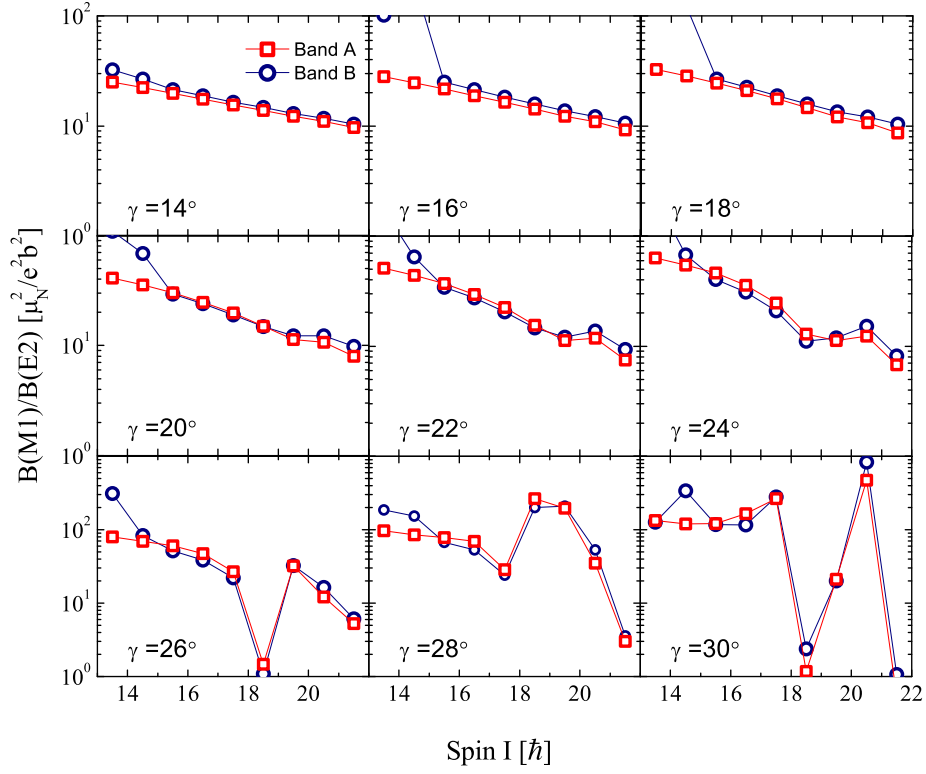


FIG. 10: (color online) The in-band $B(M1)/B(E2)$ values of the two lowest bands A and B calculated in PRM with different triaxiality parameters γ with configuration $\pi g_{9/2}^{-1} \otimes \nu h_{11/2}^2$ (open symbols).

